ASSESSMENT OF DEM ACCURACY DERIVED FROM SPOT-5 HIGH RESOLUTION STEREOSCOPIC IMAGERY

W. Kornus, R. Alamús, A. Ruiz, J. Talaya

Institut Cartogràfic de Catalunya (ICC), Parc de Montjuïc, E-08038 Barcelona
wkornus@icc.es, ralamus@icc.es, toni@icc.es, talaya@icc.es

Key words: SPOT, Space Photogrammetry, Orientation, Adjustment, DSM/DTM, Comparison, Accuracy

Summary

This paper describes the derivation of Digital Surface Models (DSMs) from 3-fold along-track stereoscopic SPOT-5 imagery in the scope of the HRS (High Resolution Stereoscopic) study, organized by the Centre Nacional d'Études Spatiales (CNES) and the International Society of Photogrammetry and Remote Sensing (ISPRS). The orientation of SPOT-5 is reconstructed by bundle adjustment using a functional model based on correction polynomials. It resulted in an RMS-error of 2 m in Easting, Northing and Height at 17 check points. DSMs are produced for 4 test sites, which are located in different terrain types (mountainous, moderate and urban). An automatic region growing image matching process generates a dense point cloud in image space, which later is rigorously transformed into the object space and converted into a regular spaced DSM. The comparison with a digital terrain model (DTM) of superior accuracy yields standard deviations better than 5 m (1σ) in flat and moderate terrain and better than 10 m (1σ) in mountainous regions. An additional DSM covering the entire image scene (approx. 60 km x 80 km) is produced with a standard deviation of approximately 8 m using the commercial software ISAE and rational functions. The sigma values include all errors of the automatic matching process as well as the differences between the surface and the terrain model and therefore must be regarded as conservative. All results are finally summarized and conclusions are drawn from the study.

1. The Spot-5 Satellite

SPOT-5 is the first satellite of the SPOT family with along-track stereo imaging capability. The two HRS cameras are tilted by +/- 20 degrees and acquire nearly simultaneous stereopairs (at a 90-second interval) of 120 km swath, along the track of the satellite, with a B/H ratio of 0.84. A continuous strip of 600 km length is covered stereoscopically with 10 m ground sampling distance (GSD) across track and with 5 m GSD along track. The nadir looking panchromatic HRG instrument provides imagery in the mono-spectral bands HMA and HMB at 5 m GSD, in the multi-spectral bands XS1, XS2, XS3 at 10 m and SWIR at 20 m GSD. The ground pixels of HMA and HMB scenes are interleaved to enable the interpolation of so-called THR 'supermode' images [1], having a nominal GSD of 2.5 m. A summary of the SPOT-5 payload and mission characteristics is given in [2]. The size of an image scene is 12000 x 12000 pixel (24000 x 24000 pixel in case of the THR 'supermode' image).

2. Initial Data

The study was conducted using an image scene covering Barcelona and the surrounding area. The data set provided by CNES comprised 5 images (HRS1, HRS2, HMA, HMB and the THR supermode image) and auxiliary data (time series of orbit positions, velocities and attitude angles, look angles for each CCD element, etc.). The ICC provided the reference data set consisting of a regular DTM of 15 m grid size and 1.1 m accuracy ($1\ \sigma_{DTM}$) covering the total area of the images and of 32 orthoimages of 0.5 m pixel size and 0.5 m accuracy ($1\ \sigma$) for 8 well distributed, approximately 10 x 14 km wide test sites (TS) (see figure 1). Figure 2 shows the two radiometrically improved and strongly reduced images of the THR and the HRS1 channels. The different resolutions of the HRS1 image in scan and flight direction are clearly visible.

3. Data Evaluation

The work flow can be subdivided into 7 steps:
1. Direct geo-referencing of the images using the supplied orientation parameters (auxiliary data)
2. Measurement of control and check points in the 8 TS
3. Mass point generation in image space using region growing matching algorithm.
4. Bundle adjustment estimating correction polynomials
5. Transformation of image mass points into object space using both strict model and rational functions
6. DSM generation using both types of data sets
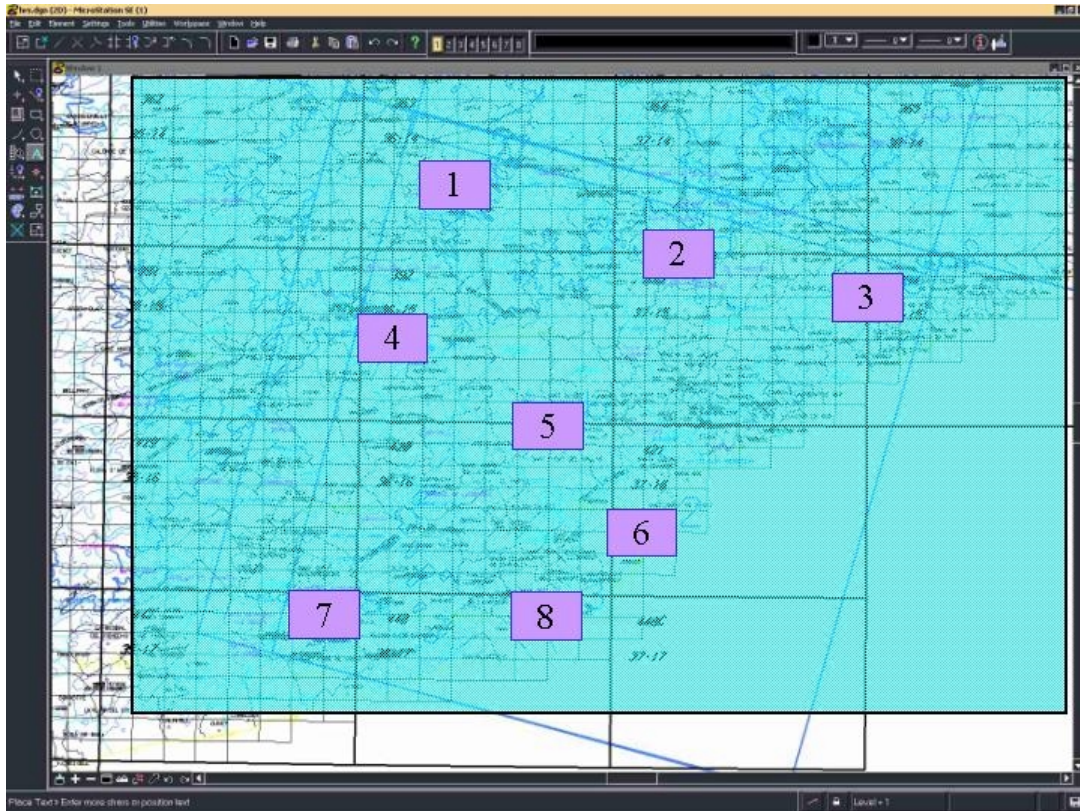7. Comparison of the DSMs with the reference DTM and statistical evaluation.

Figure 1: Location of the reference DTM (light blue rectangle) and the 8 test sites
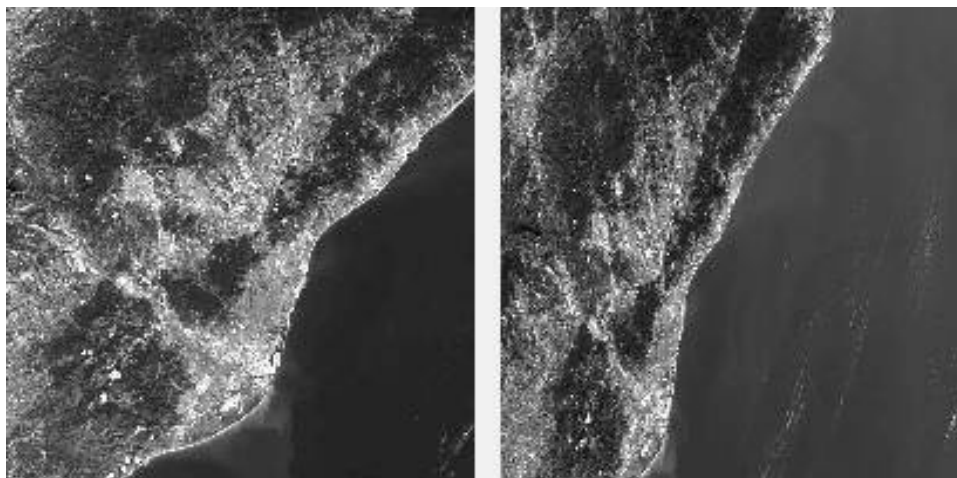

Figure 2: THR image (left, GSD: 2.5m x 2.5m) and HRS1 image (right, GSD: 10m x 5m)

3.1 Direct Geo-referencing

In a primary step the images are directly geo-referenced applying the model described in the SPOT Satellite Geometry Handbook [3] using the supplied orientation parameters and look angles. The main purpose of this step is to check the consistency and the quality of the auxiliary data. Comparing the resulting horizontal coordinates and the reference coordinates deduced from the orthoimages for a measured sample point, differences of less than 30 m are obtained which impressively demonstrates the high quality of the supplied SPOT-5 auxiliary data. The program later is extended to consider the estimated correction polynomials (see 3.4.1) and is used for the calculation of the cube data, needed for the computation of the rational functions (see 3.6)

3.2 Measurement of control and check points

It was planned to have a group of 5 points for each test site to serve either as control or as check points. They are measured by an experienced operator on a digital photogrammetric workstation with matching support in the HRS and THR images and also in the respective orthoimages. For time reasons only one of the four orthoimages per testsite is used. For a better point identification the different image scales of the HRS images are adapted applying a scale factor of 2 in scan direction. Nevertheless, the point identification resulted to be very difficult, especially in the scaled oblique looking HRS images. Only points lying on the ground surface can be selected, since the reference heights are taken from a terrain model. Due to the presence of forests and buildings in wide areas of the test sites #3, #4 and #6, there it was not possible to measure all 5 points. 19 points of the TS #1, #3, #7 and #8 are taken as control points and 17 points of the remaining TS #2, #4, #5 and #6 as check points (see figure 3).
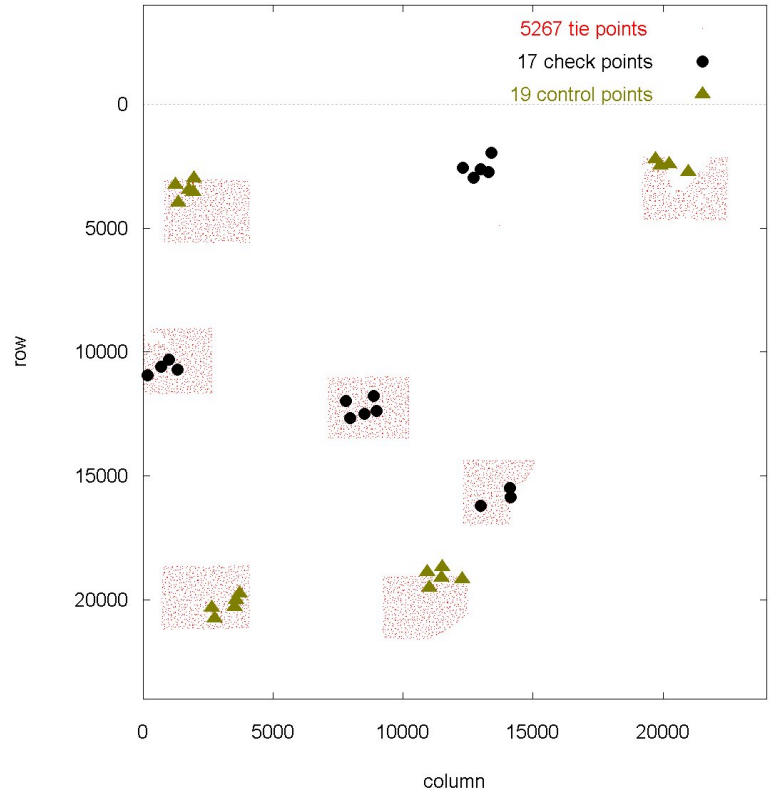

Figure 3: Location of control, check and tie points in the THR image

3.3 Mass point generation in image space

For the mass point generation in image space a modified region growing algorithm, originally developed by Otto and Chau [4], is used, which already has successfully been applied to SPOT-1 images in the early 90es [5]. Starting from a couple of manually measured so-called seed points, the algorithm matches the four neighbour pixels (left, right, upper and lower) at a given distance. For this study 1 pixel distance of the original HRS image is chosen. If the matching result meets some specified criteria (a minimum correlation coefficient, a maximum number of iterations, etc.) the point is added to a list and serves itself as a new seed point. The process ends after all points of the list are matched and no more neighbours can be found, which meet the criteria.

The algorithm is applied to sections within the 8 test site of the HRS1, HRS2 and the THR images with a size of approx. 2700 x 3300 THR pixels. For each test site 3 matching combinations are calculated: a) THR – HRS1, b) THR – HRS2 and c) HRS2 – HRS1. The THR-points successfully matched in the 1st combination are entered into the matching of the 2nd combination as so-called transfer points, i.e. only the coordinates in the second image are determined while the coordinates in the first image resulting from the previous matching run are kept. Accordingly, the resulting HRS2-points of the 2nd combination again form the transfer points of the 3rd combination. The points obtained from the 3 matching runs are classified into 3 groups, depending on the number of combination they have been matched:

1. in 1 combination (THR-HRS1 or THR-HRS2 only),
2. in 2 combinations (THR-HRS1 and THR-HRS2 or THR-HRS2 and HRS2-HRS1) and
3. in all 3 combinations.

Table 1 gives a survey of the matching results achieved in the 8 test sites. While group 1 only contains 2-ray-points, group 2 contains 3-ray-points and group 3 redundant 3-ray-points with HRS1 coordinates matched in two different matching runs. The two corresponding coordinates are averaged and deviations from the average ΔX^{S1} and ΔY^{S1} are used to calculate standard deviations $\sigma_{\Delta X}^{S1}$, $\sigma_{\Delta Y}^{S1}$. For the later DSM generation only 3-ray-points were taken with a correlation coefficient ρ bigger than 0.7 and, in case of point group 3, with deviations ΔX^{S1}, ΔY^{S1} smaller than three times their standard deviations $\sigma_{\Delta X}^{S1}$, $\sigma_{\Delta Y}^{S1}$.

From point group 3 also a subset of points is selected as input for the bundle adjustment using a regular grid of 100 x 100 pixel mesh size. Taking the point with the maximum correlation coefficient within a grid mesh, 5267 regularly distributed tie points are obtained within 7 TS (see figure 3). From TS #2 no tie points are extracted in order to serve as a real check area.

Number of Testsite	1	2	3	4	5	6	7	8
2-ray-points	75643	152505	71656	79575	119694	72379	54551	100055
2-ray-points with ρ >0.7	39108	134013	29233	57965	103744	49391	41459	88808
3-ray-points matched in 2 combinations	166657	205687	177825	170871	109805	136127	143485	137034
3-ray-points in 2 combinations with ρ > 0.7	85497	164198	58468	113097	87566	95301	82035	117369
Points matched in 3 combinations	728825	678645	467015	596486	768396	541319	797748	686262
Points in 3 combinations with $\Delta^{SI} < 3\sigma_\Delta^{SI}$	595051	601042	393743	485450	678165	454615	697439	595961
Total 3-ray-points selected for DSM generation	680548	765240	452211	598547	765731	549916	779474	713330

Table 1: Results of region growing image matching

3.4 Bundle Adjustment

In order to compensate for possible systematic errors in either the exterior orientation or/and the interior orientation data (look angles) of SPOT-5 a new functional model is implemented into ICC's adjustment software GeoTeX [6], which is described in the following. The idea behind is to estimate global correction terms of the given position and attitude of one common trajectory for all cameras and also of the given look angles for each single camera. As correction functions serve 3rd order polynomials.

3.4.1 Functional Model

The functional model is based on equation [1], which relates the look direction vector u_1 in the navigation reference frame to the look direction vector in the terrestrial coordinate frame, defined by the subtraction of the projection centre vector $[X_0, Y_0, Z_0]^T$ from the point vector $[X, Y, Z]^T$.

$$u_1 = \begin{bmatrix} -\tan(\psi_Y)_p \\ \tan(\psi_X)_p \\ -1 \end{bmatrix} = \frac{1}{\mu} R_{21}^{-1} \cdot R_{32}^{-1} \cdot \begin{bmatrix} X - X_0 \\ Y - Y_0 \\ Z - Z_0 \end{bmatrix} \qquad [1]$$

where

u_1 defines the look direction vector in the navigation reference frame. It depends on the look direction angles $(\Psi_X)_p$ and $(\Psi_Y)_p$, which are given for each pixel p of the sensor line).

R_{21} transforms the navigation reference frame into the orbital frame. It depends on the interpolated attitude angles $a_r(t)$, $a_p(t)$, $a_y(t)$ around the roll, pitch and yaw axes at time t, which are given as a time series at 8 Hz frequency.

R_{32} transforms the orbital frame into the terrestrial frame. It depends on the centre of mass position P(t) of the satellite and the velocity vector V(t), which are given as a time series at a 30 second time interval.

Eliminating the scale factor μ the applied pseudo-observation equations [2] are obtained:

$$0 = \frac{r_{11}(X - X_0) + r_{12}(Y - Y_0) + r_{13}(Z - Z_0)}{r_{31}(X - X_0) + r_{32}(Y - Y_0) + r_{33}(Z - Z_0)} - \tan(\psi_Y)_p$$

$$0 = \frac{r_{21}(X - X_0) + r_{22}(Y - Y_0) + r_{23}(Z - Z_0)}{r_{31}(X - X_0) + r_{32}(Y - Y_0) + r_{33}(Z - Z_0)} + \tan(\psi_X)_p$$

[2]

with

$$R = R_{21}^{-1}\left[a_r(t), a_p(t), a_y(t)\right] R_{32}^{-1}\left[P(t), V(t)\right] = \begin{bmatrix} r_{11} & r_{12} & r_{13} \\ r_{21} & r_{22} & r_{23} \\ r_{31} & r_{32} & r_{33} \end{bmatrix} \qquad [3]$$

The coefficients of the correction polynomials are the actual unknowns of the adjustment, which are applied to the parameters of the external orientation E_t (equation [4]), i.e. to the position vector $P(t)=[X_0, Y_0, Z_0]^T$ and to the attitude angles $a_r(t)$, $a_p(t)$, $a_y(t)$ as well as to the parameters of the internal orientation I^S_p (equation[5]), i.e. to the look direction angles $(\Psi_X)_p$ and $(\Psi_Y)_p$ of sensor line S and pixel p.

$$E = E_t + \hat{A}_E + \hat{B}_E(t-t_c) + \hat{C}_E(t-t_c)^2 + \hat{D}_E(t-t_c)^3 \qquad [4]$$

$$I^S = I^S_p + \hat{A}^S_I + \hat{B}^S_I(\frac{p-p_c}{1000}) + \hat{C}^S_I(\frac{p-p_c}{1000})^2 + \hat{D}^S_I(\frac{p-p_c}{1000})^3 \qquad [5]$$

The external orientation parameters E (equation [4]) enter in the equations [2] and [3]. They are derived from the interpolated parameter E_t at time t of the corresponding image line and the 3rd order correction polynomial with its unknown coefficients A_E, B_E, C_E and D_E. t_C here is defined as time of the central line (#12001) of the THR image. The internal orientation parameters I^S (equation [5]) also enter in equation [2]. They are derived from the parameter I_p^S of the interpolated sensor position p and the 3rd order correction polynomial with its unknown coefficients A_I^S, B_I^S, C_I^S and D_I^S. p_C here is defined as the centre pixel of the respective sensor line S.

This model involves 48 unknowns, if 3 viewing directions are involved (like in this evaluation: HRS1, HRS2 and THR), i.e. 4 unknowns for each of the 6 external orientation parameters and 2 x 4 unknowns for each of the 3 sensor lines. In practice only a subset of these 48 unknowns will be significantly determinable and the rest of the parameters need to be fixed in order to avoid over-parametrization problems.

3.4.2 Input

The following observations are introduced into the adjustment:
− Image coordinates of 19 control and 17 check points (σ=0.5 pixel), measured in the HRS1, HRS2 and the THR images (see figure 3),
− image coordinates of 5270 tie points, obtained by automated image matching in the HRS1, HRS2 and the THR images (σ = 0.5 pixel, see figure 3),
− horizontal object coordinates of 19 control points (σ = 2.5 m, corresponding to the ground sample distance of the THR-channel, which is limiting the point identification accuracy),
− heights of 19 control points (σ = 2.2 m = 2 x σ_{DTM}).

The supplied look angles, ephemeris, velocity and attitude parameters enter as constants and not as observations.

3.4.3 Results

In order to get rid of correlation effects between external and internal orientation, the 24 CPC for the external orientation parameters were fixed in a first step and only 24 CPC for the look angles are estimated. Later in a second step, i.e. after the set of significantly determinable CPC (for the look angles) has been found, this set together with the 24 CPC for the external orientation parameters are estimated simultaneously.

3.4.3.1 Bundle adjustment using HRS and HRG data

In a series of adjustment runs those CPC are consecutively fixed, whose estimated values are small compared to their estimated standard deviations. Simultaneously it is monitored, whether the fixing of the CPC provokes a systematic alignment or an increase of the residual vectors of the control points both in image and in object space. If there is an increase or a systematic, the CPC is not fixed, even if the relation between value and standard deviation is small. After a series of adjustment runs it turned out, that 15 of the 24 CPC can be fixed and consequently 9 CPC are determined more or less significantly. In table 2 their estimated values (x), the estimated standard deviations (σ_x), their significance (x/σ_x) and the maximum effect (E) in pixel at the edges of the CCD-array are listed.

Table 3 shows the statistics on the differences of the coordinates at the 17 check points, indicating an empirical error of approximately 2 meters in Easting (dE), Northing (dN) and Height (dH). Table 4 lists the statistics on the differences between the 5235 estimated tie point heights and their interpolated DTM heights. The respective histogram is shown in figure 4. The higher frequency of positive height differences is due to tie points lying on top

of the vegetation or artificial objects, which actually must not be compared directly to the DTM heights. If these points would be filtered out, the statistics would improve.

Channel		A_x	B_x	C_x	D_x	A_y	B_y	C_y	D_y
THR	x	5.3E-06	1.0E-06			2.8E-05			
	σ_x	7.8E-06	1.1E-07			3.3E-06			
	x/σ_x	0.7	9.9			8.6			
	E	1.8	4.2			9.5			
HRS1	x	-4.9E-06				1.5E-05		-4.2E-07	-6.9E-08
	σ_x	1.3E-05				5.6E-06		4.7E-07	9.1E-08
	x/σ_x	0.4				2.6		0.9	0.8
	E	-0.4				2.4		-2.6	-2.5
HRS2	x							-4.6E-07	-7.4E-08
	σ_x							4.8E-07	9.6E-08
	x/σ_x							1.0	0.8
	E							-2.8	-2.6

Table 2: Estimated correction polynomial coefficients for look angles (x), standard deviations (σ_x), significance (x/σ_x) and maximum effect (E) [pixel]. A_x-D_x apply in scan direction, A_y-D_y in flight direction

	MIN.	MEAN	MAX.	RMS.	σ [m]
dE	-4.40	-2.07	1.39	2.67	1.74
dN	-6.06	0.81	3.68	2.33	2.25
dH	-4.43	0.19	2.46	1.90	1.95

Table 3: Statistics on coordinate differences of the 17 check points

	MIN.	MEAN	MAX.	RMS.	σ [m]
dH	-22.24	2.10	63.30	6.11	5.74

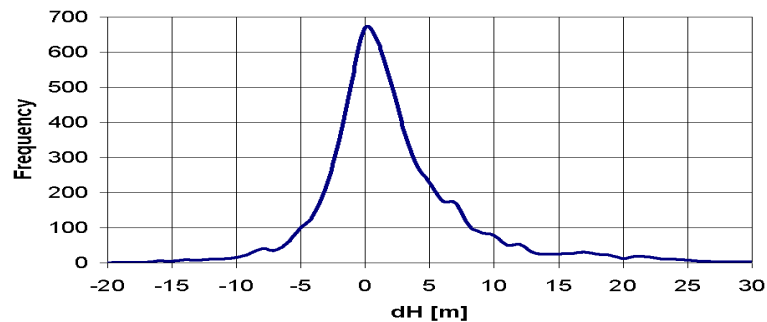Table 4: Statistics on height differences between 5235 tie points and the reference DTM

Figure 4: Histogram of height differences between tie points and the reference DTM

The adjustment employing also CPC for the position and attitude parameters in addition to the 9 CPC for the look angles did not show a significant improvement. Thus, it was concluded not to correct the attitude and position parameters, i.e. to apply the 9 estimated CPC to the look angles only.

3.4.3.2 Bundle adjustment using HRS data only

HRG imagery is not available for all SPOT5 stereo data sets. Therefore an additional adjustment is done considering pure SPOT-5 HRS data. It turned out, that without HRG data none of the CPC can be determined significantly. This is not that astonishing, since the effect of the estimated CPC for the HRS1 and HRS2 channels proved to be very small (less than 3 pixels maximum, see table 2). Consequently, an adjustment with all CPC fixed to value 0 was calculated, whose results are listed in tables 5 and 6:

	MIN.	MEAN	MAX.	RMS.	σ [m]
dE	-5.02	-1.69	6.10	3.82	3.52
dN	-5.02	0.54	5.13	2.92	2.96
dH	-2.76	0.96	4.17	2.08	1.90

Table 5: Statistics on coordinate differences of 17 check points after adjustment of HRS data only, all CPC fixed

	MIN.	MEAN	MAX.	RMS.	σ [m]
dH	-22.07	2.65	60.35	6.61	6.05

Table 6: Statistics on height differences between 5233 tie points and reference DTM after adjustment of HRS data only, all CPC fixed

From the analysis of other three-line-scanner imagery as e.g. the German MOMS-02 camera we already know, that the presence of a nadir view primarily improves the horizontal accuracy and does not directly affect the height accuracy [7]. This also can be observed comparing the results of the tables 5 and 6 with the tables 3 and 4. The statistics on the height differences remains more or less the same, while the horizontal differences at the 17 check points increase - but still remain far better than 1 pixel.

3.5 DSM by strict model

After the adjustment the imaging geometry is known and image points can rigorously be transferred into object space using the estimated internal and external orientation parameters. From the resulting 3D mass point cloud TIN models are produced, which later are exported into 10 m raster DSMs.

3.5.1 Mass point cloud transformation into object space

The mass point cloud is transformed point-wise into object space by a local adjustment based on equation [6], which is the inverse form of equation [1] using the estimated model parameters listed in table 2. For each point and image 3 equations are defined:

$$X = X_0 + \mu \cdot R_{32} \cdot R_{21} \cdot (u_1)_X$$
$$Y = Y_0 + \mu \cdot R_{32} \cdot R_{21} \cdot (u_1)_Y \qquad [6]$$
$$Z = Z_0 + \mu \cdot R_{32} \cdot R_{21} \cdot (u_1)_Z$$

Using the X, Y, Z object coordinates and the scale factor μ as unknowns, 9 equations are formulated to solve for 6 unknowns $(X,Y,Z,\mu_1,\mu_2,\mu_3)$ in the case of 3-ray-points, and 6 equations for 5 unknowns (X,Y,Z,μ_1,μ_2) in the case of 2-ray-points. The transformation is executed separately for the above mentioned 3 point groups: 2-ray-points, 3-ray-points matched in 2 and in 3 combinations. The test sites #1, #3, #7 and #8, which contain control points are excluded from the following accuracy assessment.

3.5.2 Comparison with the reference DTM

After the transformation the height coordinates are compared to the reference DTM heights, which previously have been interpolated for the respective horizontal coordinates. In figure 5 the height differences of the mass points for TS #5 are depicted in a color coded representation:

- blue: dh < -5m
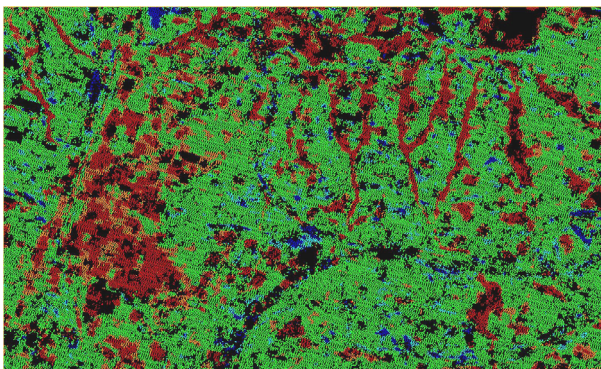- light blue: -5m < dh < -3 m
- green: -3m < dh < 3m
- orange: 3m < dh < 5m
- red: dh > 5m

Figure 2: Color coded height differences between points and reference DTM for TS #5 (section: 5.3x3.6 km^2)

Figure 6:Orthoimage of TS #5 (section: 5.3 x 3.6 km^2)

As can be seen, the matching algorithm works quite well, if the image contains sufficient contrast and texture. On the other hand, in those parts with poor contrast and/or texture the matching failes, causing gaps in the 3D point cloud and, consequently, in the DSM. In the orthoimage in figure 6 the pointless areas can clearly be identified as

areas with low contrast (like the wide road in the central lower image part) or homogeneous texture (like the forest in the upper right corner of the image). It also can be seen, that red points, indicating height differences bigger than 5m, mainly appear in the urban area in the left part of the image or in forest zones, e.g. in the upper right image part. This illustrates well the difference between the surface model deduced from the point cloud and the reference terrain model representing the bare Earth's surface. Table 7 shows statistics of the complete comparison between point heights and reference DTM.

The results are derived from the complete unfiltered sets of the automatically matched points, including blunders and points on top of vegetation and buildings. For time reasons no filtering or editing was done. In this respect, the RMS values must be interpreted as conservative with a considerable potential for improvement. Since TS #6 covers the Barcelona urban area and contains only few ground points, the accuracy potential of SPOT5 should rather be deduced from the results of the other test sites #2, #4 and #5.

TS	N	Min	Mean	Max	RMS	σ
#2	601042	-27.5	0.3	30.2	3.8	3.8
#4	485450	-85.5	0.3	88.0	5.2	5.1
#5	678165	-49.4	1.5	33.5	4.0	3.7
#6	446380	-39.7	10.9	66.9	13.0	7.2
Point group 1: 3-ray-points from 3 matching runs						
#2	164411	-69.1	0.1	56.3	4.1	4.0
#4	119301	-142.2	1.6	165.4	11.6	11.4
#5	86635	-109.0	1.1	99.0	5.1	5.0
#6	68979	-106.7	8.1	95.9	12.4	9.4
Point group 2: 3-ray-points from 2 matching runs						
#2	134013	-175.3	0.1	99.8	5.4	5.4
#4	57965	-141.1	1.7	203.6	13.8	13.7
#5	103744	-223.6	1.3	226.3	6.0	5.9
#6	35571	-151.6	6.6	151.9	12.4	10.6
Point group 3: 2-ray-points						

Table 7: Statistics on height differences dh [m] between the 3D object points and the reference DTM

The points matched in 3 combinations yield, as expected, the best results with RMS height differences of about 4 m in the moderate terrain of the TS #2 and #5 and of about 5 m in the mountainous terrain of TS #4. There also exist some blunders with differences up to nearly 90 m. 3-ray-points matched in 2 combinations lead to acceptable 4-5 m height differences in moderate terrain. In mountainous terrain, however, the RMS differences increase to nearly 12 m and the blunders to more than 160 m. For 2-ray-points this situation is even worse. In figure 7 the histogram of the height differences for TS #5 is depicted as an example separately for the 3 point groups.
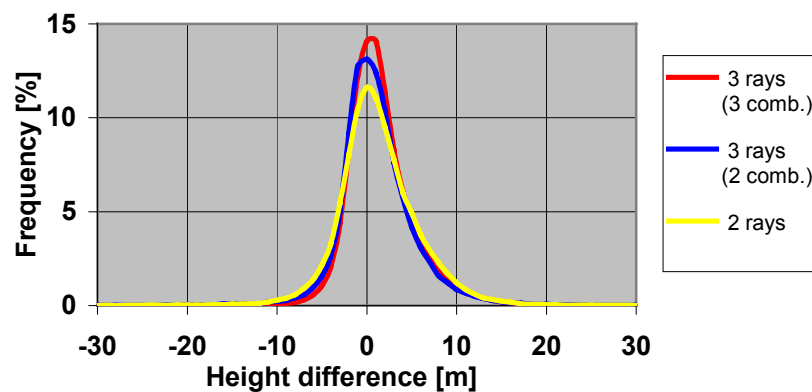

Figure 7: Histogram of height differences dh [m] for TS #5

Table 8 shows the respective statistics on height differences obtained from a pure HRS data set without considering the HRG data. This implies new matching runs without transfer points (see section 3.3) and also no estimation of correction polynomial coefficients (see section 3.4.3.2); i.e. the matched image points are directly transferred into object space using the supplied auxiliary data and the local adjustment described in section 3.5.1. The standard deviation are approximately 20% worse compared to the results achieved with bundle adjustment and matching in 3

combinations (see table 7). Additionally a systematic height error of approximately 9 m occurs, which still is subject to further investigation since the results of the bundle adjustment did not show a comparable systematic effect (see tables 5 and 6)

TS	N	Min	Mean	Max	RMS	σ
#2	997949	-63.4	8.6	121.2	9.8	4.7
#4	940159	-155.1	9.1	288.3	14.0	10.7
#5	956022	-100.5	9.6	75.9	10.6	4.6
#6	575775	-131.7	18.6	154.1	21.1	9.9

Table 8: Statistics on height differences dh [m] between the 3D object points derived from HRS data only and the reference DTM

It was stated above, that the nadir looking view of the HRG channel does not contribute very much to the height accuracy. This is true from the geometric point of view in the case of well identifiable check points. Here, in the case of the automated mass point generation process by image matching we can see, that the third view considerably improves the results in terms of accuracy and reliability, especially in mountainous regions.

3.6 DSM by rational functions

As a second method of DSM generation rational functions are employed. Two sets of 1331 equally distributed points per image are transformed into object space; one for the HRS/HRG data using the 9 estimated correction parameters (see 3.4.3.1), the other using pure HRS data without applying correction polynomials (see 3.4.3.2). The points are equally distributed in a cube, defined by increments of 1200 pixels in image columns and rows and by increments of 250 m in object height (from −250 m to 2250 m). From these points the best coefficients of the rational functions are determined by least squares adjustment. For forward and backward looking directions rational functions of degree 3 in numerator and denominator are used. In case of the nadir looking direction a 3rd order polynomial is adjusted, since it has not been possible to adjust any polynomial denominator without zeros in the domain of the image footprint.

3.6.1 Matching in image space (region growing)

In a first step the rational functions are used, as an alternative to the strict model, to transform the image points, matched in 3 combinations using the region growing algorithm (see above) into object space. The statistics on the height differences between the resulting object coordinates and the coordinates computed with the strict model are listed in table 9. The difference turned out to be not significant and confirms the findings of an earlier analysis using MOMS-02 images, where it was concluded that stereoplotting with rational functions is as accurate as using a rigorous model [8]. Therefore, no new DSM are produced, i.e. it is assumed, that this rational function approach is also represented by the strict model DSMs.

TS	N	Min	Mean	Max	RMS	σ
#2	601041	-9.3	-0.6	15.7	0.6	0.2
#4	485449	-16.6	-0.3	18.1	0.5	0.3
#5	678164	-8.5	-0.4	14.8	0.5	0.2

Table 9: Statistics on height differences [m] between the points, matched in 3 combinations, derived from rational functions and from the strict model

3.6.2 Matching in object space (ISAE)

In a further step the commercial software ISAE [9] is used, which applies feature based matching in object space. Two DSMs are generated from HRS1 and HRS2 images using two different sets of rational functions. The first one is deduced from the data cube sets derived from HRS/HRG using the 9 estimated correction parameters and the second one from pure HRS data without applying correction polynomials. A grid step of 45 m and an a priory accuracy of 2.5 m is selected. In both DSMs more than 17 millions of matching points with more than 5 points per mesh are found. An internal height accuracy of 0.9 m is obtained for the first DSM and 1.3 m for the second, which proved to be too optimistic compared to the empiric quality measures presented in the next section.

4. Assessment of generated DSM

Table 10 lists the statistics on the height differences dh' between the DSM raster point heights (10 m grid) and the reference DTM. In addition to the pure point errors dh listed in table 7, these dh' values also include the DSM interpolation error. Without considering the HRG data the standard deviations for the TS #2 and #5 located in moderate terrain deteriorate only about 10% compared to the results achieved with HRG and bundle adjustment in addition to the already mentioned systematic height error of 9 m. In the mountainous terrain of test area #4 the results deteriorate about 60%, which again underlines the importance of the third view in mountainous terrain, at least for this DSM generation method applying region growing image matching.

TS	N	Min	Mean	Max	RMS	σ
#2	510531	-66.5	0.7	49.7	4.5	4.4
#4	424112	-124.5	1.1	125.7	9.3	9.2
#5	478139	-106.5	1.6	95.6	4.6	4.3
HRS/HRG data, 9 estimated CFC						
#2	507413	-60.8	8.8	101.9	10.1	4.9
#4	413740	-151.9	9.3	280.5	17.2	14.4
#5	476494	-95.5	9.8	71.5	10.9	4.7
HRS data, no bundle adjustment						

Table 10: Statistics on height differences dh' [m] between the DSM raster points (10m grid) obtained with region growing image matching and the reference DTM

Figure 8 shows the DSM of the entire image scene at 45 m grid size derived with ISAE. The corresponding statistics on the height differences dh' is listed in table 11. Without considering the HRG data the results deteriorate about 10%, in the mountainous terrain of TS #4 even 45%. Compared to the results in table 10 the results are 20-25% worse. The standard deviation for the full scene is 8-9 m.

TS	N	Min	Mean	Max	RMS	σ
#2	25625	-41.4	0.7	78.81	5.4	5.3
#4	21445	-96.9	2.2	107.3	11.7	11.5
#5	24322	-33.0	1.9	32.5	5.4	5.1
Full scene	1576146	-143.4	1.7	185.4	8.4	8.3
HRS/HRG data, 9 estimated CFC						
#2	25625	-67.3	1.7	150.4	5.9	5.7
#4	21445	-135.2	4.1	338.6	17.2	16.7
#5	24322	-144.9	3.0	119.9	6.5	5.8
Full scene	1579054	-423.0	3.0	457.4	9.7	9.2
HRS data, no bundle adjustment						

Table 11: Statistics on height differences dh' [m] between the DSM raster points (45 m grid) derived from ISAE and the reference DTM

5. Summary and conclusion

This report describes the DSM generation using SPOT5 HRS and HRG-supermode images. Correction polynomials for the provided look angle values of each camera (interior orientation) are estimated by bundle block adjustment using 17 ground control points in 4 control areas located in the 4 corners of the covered surface. The application of correction polynomials for position and attitude (exterior orientation) proves to be not necessary. The bundle adjustment results in a point accuracy of 2 m in Easting, Northing and Height, which is demonstrated by 17 independent check points, distributed in 4 check areas.

An automated region growing image matching algorithm is applied to generate mass points in image space, which later are transformed into object space. Without manual editing and/or filtering of the resulting point cloud an RMS height error of approximately 4 m (5 m in mountainous terrain) is obtained for 3-ray-points matched in 3 combinations (nadir-backward, nadir-forward, backward-forward). For 3-ray-points matched in 2 combinations and for 2-ray-points the RMS error is worse especially in mountainous areas. It turns out, that the point cloud of the applied matching process can be produced automatically with sufficient density in wide parts, but not in all parts of the images. The algorithm fails in areas with poor image contrast and/or homogenous texture like forests, broad streets, large agricultural areas, etc. Here manual interaction is required in order to avoid gaps in the point cloud

and, consequently, in the produced DSM. This part of the work flow can be rather time consuming and therefore has been excluded from that study. In other words, the presented results reflect the accuracy potential of SPOT-5 HRS which can be achieved by largely automatic processing and which still can be improved to some extent by manual effort.
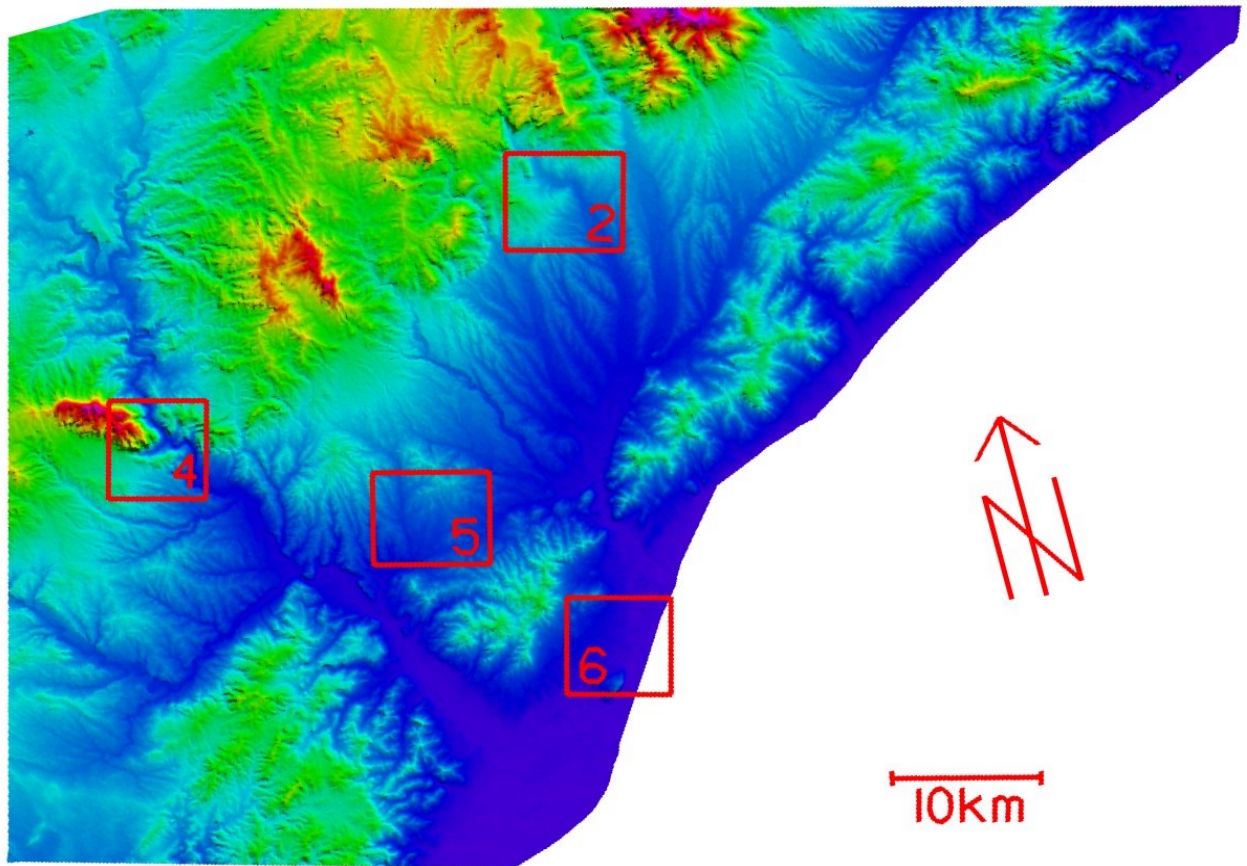

Figure 8: Color coded DSM representation of the entire image scene (approx. 80 km x 60 km), generated by ISAE using the HRS1 and HRS2 channels at 45 m grid size. The location of the four check areas is marked in red.

Figure 9 gives a summary of the obtained standard deviations of the height differences between the produced DSMs and the reference DTM. As can be seen, they depend on the terrain type, on the number of employed viewing directions (cameras) and on the used method, which leads to the following 3 simple statements: 1. The DSM accuracy in mountainous terrain is lower than in moderate and flat terrain, which is obvious due to the higher probability of occlusions and due to the higher impact of horizontal errors. In addition, homogenous image patterns, e.g. in forest areas, which also obstruct the matching process, produce gaps in the point cloud and later in the DSM. Here is the biggest potential of accuracy improvement by manual interaction. 2. Three viewing directions (HRS/HRG) are better than two (HRS only). Although the nadir viewing camera HRG does not geometrically contribute to a better height accuracy, its presence, however, supports the accuracy and reliability of the matching process, especially in mountainous regions, where it also helps to bridge occlusions. Nevertheless, HRG imagery, if available at all, does not cover the whole HRS scene and therefore it is not always possible to use a three viewing (HRS/HRG) approach. 3. The DSM generated with region growing image matching are more accurate than the ISAE-DSM, which probably is at least partly due to the different grid spacing. The actual reasons have not been analysed in this study.

The study demonstrates, that DSM production using SPOT-5 data is possible with an absolute accuracy of better than 5 m (1σ). In mountainous areas the accuracy is worse due to occlusions obstructing the automated mass point generation process, especially if no nadir viewing HRG imagery is available. The presented results still include all errors of the automatic matching process and also the difference between the produced surface model and reference terrain model. Therefore it is expected, that the accuracy values still can be considerably improved by manual editing and appropriate filtering, filling the gaps in the automatically generated point cloud and excluding blunders and points on top of vegetation or artificial objects.
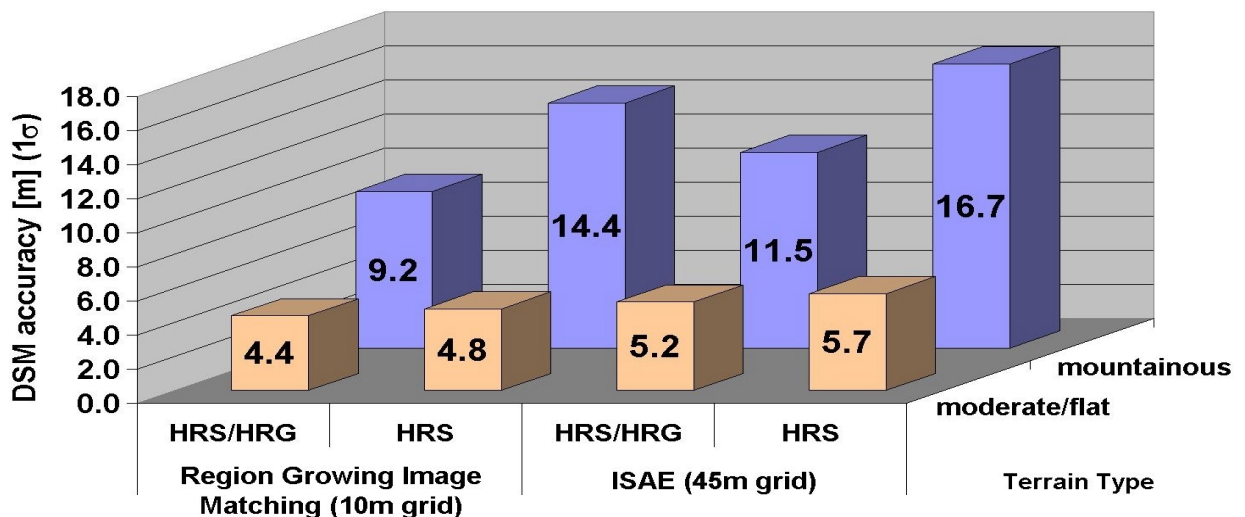
Figure 9: Summarized standard deviations of height differences between the produced DSMs and reference DTM

References

[1]   SPOT Magazine No. 31, 2000: "*The secrets of SPOT-5 Supermode*", Sept. 2000.

[2]   Fratter C., Moulin M., Ruiz H., Charvet P., Zobler D., 2001: "*The SPOT-5 Mission*", 52nd International Astronautical Congress, Toulouse, France.

[3]   SPOT Image, 2002: "*SPOT Satellite Geometry Handbook, S-NT-73_12-SI, Edition 1, Revision 0*", 15. 01. 2002

[4]   Otto G., Chau T., 1989: "*Region growing algorithm for matching of terrain images*", Image and vision computing (7) 2, pp. 83-94.

[5]   Heipke C., Kornus W., 1991: "*Nonsemantic photogrammetric processing of digital imagery – the example of SPOT stereo scenes*" in: Ebner, Fritsch, Heipke (Eds.): Digital Photogrammetric Systems, ISBN 3-87907-234-5, Wichmann Verlag Karlsruhe, Germany, pp. 86-102.

[6]   Colomina, I., Navarro, J., Térmens, A.,1992: "*GeoTeX: a general point determination system*", International Archives of Photogrammetry and Remote Sensing, Vol. 29, Comm. III, pp. 656--664, Washington D.C, USA.

[7]   Ebner H., Kornus W., Ohlhof T., 1992: „*A simulation study on point determination for the MOMS-02/D2 space project using an extended functional model*", International Archives of Photogrammetry and Remote Sensing, Vol. 29, B4, pp. 458-464, Washington D.C, USA.

[8]   Alamús R., Kresse W., Langner M., 2000: "*Accuracy potential of point measurements in MOMS-images using a rigorous model and a rational function*". International Archives of Photogrammetry and Remote Sensing, Vol. 33, B4, pp. 515-517, Amsterdam, The Netherlands.

[9]   Krzystek P., 1991: "*Fully Automatic Measurement of Digital Elevation Models*", Proceedings of the 43th Photogrammetric Week, Stuttgart, pp. 203-214.